ChemPubSoc Europe

DOI: 10.1002/ejic.202000041

EurJIC European Journal of Inorganic Chemistry

Full Paper

Ammonothermal Synthesis

Ammonothermal Synthesis of Ba_2PO_3N – An Oxonitridophosphate with Non-Condensed PO_3N Tetrahedra

Sebastian Wendl,[a][‡] Mathias Mallmann,[a][‡] Philipp Strobel,[b] Peter J. Schmidt,[b] and Wolfgang Schnick*[a]

Abstract: The *ortho*-oxonitridophosphate Ba_2PO_3N was synthesized under ammonobasic conditions (T = 1070 K, p = 120 MPa) in custom-built high-temperature autoclaves, starting from red phosphorus, BaO, NaN_3 and KOH. Thus, single crystals of up to several hundred µm were obtained, which were used for single-crystal X-ray diffraction. Ba_2PO_3N [*Pnma* (no. 62), a = 7.596(2), b = 5.796(1), c = 10.212(3) Å, Z = 4] crystallizes in the β-K_2SO_4 structure type with non-condensed $[PO_3N]^{4-}$ ions and is isotypic to its lighter homologues EA_2PO_3N (*EA* = Ca, Sr). Powder X-ray diffraction, energy dispersive X-ray and Fourier Transformed Infrared spectroscopy corroborate the crystal structure. The optical band gap was determined by means of diffuse reflectance UV/Vis spectroscopy to be 4.3 eV. Eu^{2+} doped samples show green luminescence (λ_{em} = 534 nm, fwhm = 85 nm/2961 cm^{-1}) when irradiated with UV light (λ_{exc} = 420 nm). However, $Ba_2PO_3N:Eu^{2+}$ shows strong thermal quenching, even at room temperature.

Introduction

During the 1960s, Jacobs and co-workers developed the ammonothermal method, in which supercritical ammonia is used as solvent and nitrogen source for the synthesis of various imides, amides and nitrides.[1–6] Thereby, supercritical ammonia facilitates the crystallization process, as it increases the solubility of the inorganic starting materials, which are quite insoluble in liquid ammonia.[7,8] With the first synthesis of GaN in supercritical ammonia in 1995, the ammonothermal approach was established as important method for synthesis and crystal growth of high-quality GaN crystals.[9–11] Subsequently, the ammonothermal approach turned out as a promising route for explorative synthesis of different (oxide) nitrides such as wurtzite-type Grimm–Sommerfeld analogous nitrides [e.g. InN, II-IV-N_2 (II = Mg, Mn, Zn; IV = Si, Ge), $CaGaSiN_3$ or $Ca_{1-x}Li_xAl_{1-x}Ge_{1+x}N_3$ ($x \approx 0.2$)] and oxide nitride perovskites [e.g. $EAMO_2N$ (*EA* = Sr, Ba; *M* = Nb, Ta)] as well.[12–18] Most recently, the syntheses of numerous nitridophosphates with different degrees of condensations κ (i.e. atomic ratio of tetrahedra centers to ligand) could be realized. Here, a great structural diversity ranging from non-condensed tetrahedra groups up to network structure types, exhibiting values for κ from 1/3 to 4/7, was observed.[19–21] Compared to other synthetic methods towards nitridophosphates, such as condensation reactions, synthesis in pressure ampoules or high-pressure synthesis using the multi-anvil technique, the ammonothermal method exhibits significant advantages.[22] This includes the prevention of thermal decomposition of the target compounds, the use of simple starting materials including red phosphorus (P_{red}) as well as large sample volumes for a detailed characterization of their materials properties.[21]

However, there is no ammonothermally synthesized *ortho*-(oxo)nitridophosphate showing non-condensed $[PO_{4-x}N_x]^{(3+x)-}$ tetrahedra, up to now. Such structural features were only observed in Li_7PN_4, $Li_{14}[PON_3]_2O$, EA_2PO_3N (*EA* = Ca, Sr) and $Ho_3[PN_4]O$, which were synthesized in ampoules or via high-pressure synthesis, respectively.[23–26] Especially, the EA_2PO_3N compounds are of special interest, as they crystallize isotypically to β-K_2SO_4. Accompanied with a plethora of compounds crystallizing in this structure type, a great diversity of materials properties is observed. Especially, the potential as host lattices for luminescent materials is impressive, covering the whole visible spectrum from red ($LaEASiO_3N:Eu^{2+}$ with *EA* = Sr, Ba) over green ($Ca_2PO_3N:Eu^{2+}$) to blue ($KSrPO_4:Eu^{2+}$) emission.[25,27,28]

In this contribution, we present the ammonothermal synthesis of the *ortho*-oxonitridophosphate Ba_2PO_3N containing discrete $[PO_3N]^{4-}$ ions, extending the degree of condensation range of ammonothermally accessible nitridophosphates to $1/4 \le \kappa \le 4/7$. The structure was elucidated using single-crystal X-ray diffraction on ammonothermally grown crystallites with sizes up to several hundreds of µm. Bulk samples were used for further analysis as well as for examination of luminescence properties of Eu^{2+} doped Ba_2PO_3N. Together with earlier re-

[a] *Department of Chemistry, University of Munich (LMU), Butenandtstraße 5-13 (D), 81377 Munich, Germany*
E-mail: wolfgang.schnick@uni-muenchen.de
https://www.cup.lmu.de/ac/schnick/
[b] *Lumileds Phosphor Center Aachen, Lumileds Germany GmbH, Philipsstraße 8, 52068 Aachen, Germany*
[‡] S.W. and M.M.: These authors contributed equally to this work.
Supporting information and ORCID(s) from the author(s) for this article are available on the WWW under https://doi.org/10.1002/ejic.202000041.

ported investigations on the ammonothermal approach, this work demonstrates once again the high potential of this method regarding synthesis and crystal growth of (oxide) nitride materials.

Results and Discussion

Synthesis

The oxonitridophosphate Ba_2PO_3N was synthesized ammonothermally using custom-built high-temperature autoclaves made of the nickel-based super-alloy Haynes® 282®. Stoichiometric amounts of P_{red} and BaO were used as starting materials. KOH and NaN_3 were added as additional oxygen and nitrogen sources as well as ammonobasic mineralizers. They form in situ $NaNH_2$ and KNH_2, which increase the solubility of the other starting materials by the formation of soluble intermediate species, such as mixed amides [e.g. $KBa(NH_2)_3$] and phosphorus containing compounds like hexaaminocyclotriphosphazene $[PN(NH_2)_2]_3$, the corresponding ammoniate $[PN(NH_2)_2]_3{\cdot}0.5NH_3$ or the imidonitride $Na_{10}[P_4(NH)_6N_4](NH_2)_6(NH_3)_{0.5}$.[3,7,21,29–31] When using NaOH instead of KOH, Ba_2PO_3N appears only as side-phase without any single crystals of significant size. The remaining PXRD reflections could not be assigned to any known compound. A possible explanation could be the non-existence of a Na analog to $KBa(NH_2)_3$, resulting in a lower solubility.

Based on the observation that such intermediates are preferably formed at low temperatures, the reaction mixture was heated in a first step to a temperature of 670 K. After 16 h the autoclave was subsequently heated to 1070 K, reaching a pressure of 120 MPa, in order to transform the intermediate species into the oxonitridophosphate Ba_2PO_3N. Upon adding $Eu(NH_2)_2$ to the starting materials, the product exhibits green luminescence (see Luminescence section). To prevent the product from autoclave impurities, the reaction mixture was filled into a Ta-liner. In addition, the liner wall acted as a substrate for single-crystal growth of the product. Thereby, single crystals with sizes up to ≈ 600 µm were accessible. Figure 1 illustrates ammonothermally grown crystals of $Ba_2PO_3N:Eu^{2+}$. The size of the crystals, which are up to several hundred µm, as well as the fact that the crystals grew on the wall at the upper part of the liner, which is supposed to be the colder zone, suggest a solution based transport and growth mechanism via intermediate species.

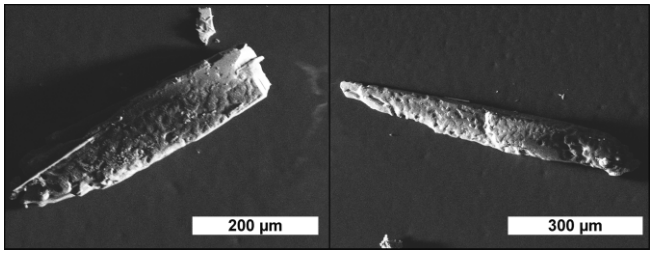

Figure 1. SEM images of $Ba_2PO_3N:Eu^{2+}$ crystals.

The obtained white (Ba_2PO_3N) and yellow ($Ba_2PO_3N:Eu^{2+}$) products are slightly sensitive towards moisture and were therefore washed with dry ethanol to eliminate hygroscopic residual mineralizer and intermediate species.

Crystal Structure

The crystal structure of Ba_2PO_3N was solved and refined from single-crystal X-ray diffraction data in the orthorhombic space group *Pnma* (no. 62) with lattice parameters a = 7.596(2), b = 5.796(1) and c = 10.212(3) Å. The crystallographic data are summarized in Table 1. Wyckoff positions and atomic coordinates, anisotropic displacement parameters, as well as interatomic distances and angles are given in Tables S1–S3 (Supporting Information). Ba_2PO_3N crystallizes in the β-K_2SO_4 structure type and is isotypic to its lighter homologues Ca_2PO_3N and Sr_2PO_3N.[25] As expected, the lattice parameters of the three EA_2PO_3N compounds increase linearly with increasing size of the alkaline earth ions (see Figure S1, Supporting Information). The crystal structure is built up from non-condensed $[PO_3N]^{4-}$ tetrahedra (see Figure 2) and therefore exhibits a degree of condensation of $\kappa = n(P)/n(O,N) = 1/4$, which expands the range of ammonothermally accessible degrees of condensation for (oxo)nitridophosphates to $1/4 \leq \kappa \leq 4/7$. The assignment of O and N atoms was carried out in accordance with the structure model of EA_2PO_3N (*EA* = Ca, Sr).[25] Lattice energy calculations (MAPLE),[32–35] bond-valance sums (BVS)[36,37] as well as charge distribution (CHARDI)[38] calculations support the ordering and show only slight deviations from expected values (see Tables S4–S6, Supporting Information). The P–O [1.573(2)–1.602(2) Å] and P–N distances [1.578(2) Å] are in good agreement with bond lengths of other alkaline earth oxonitridophosphates known from literature (e.g. Ca_2PO_3N, Sr_2PO_3N, SrP_3N_5O,

Table 1. Crystallographic data of Ba_2PO_3N obtained from single-crystal X-ray diffraction.

Formula	Ba_2PO_3N
Crystal system	orthorhombic
Space group	*Pnma* (no. 62)
Lattice parameters /Å	a = 7.596(2)
	b = 5.796(1)
	c = 10.212(3)
Cell volume /Å^3	449.6(2)
Formula units/cell	4
Density /g cm^{-3}	5.4325
Crystal size /mm^3	0.01 × 0.03 × 0.04
μ /mm^{-1}	17.640
T /K	296(2)
Diffractometer	Bruker D8 Quest
Radiation (λ /Å)	Mo-K_α (0.71073)
F (000)	632
θ range /°	3.343 - 35.687
Total no. of reflections	15148
No. of independent reflections	1121
Observed reflections [$F^2 > 2\sigma(F^2)$]	1029
R_{int}; R_σ	0.0432; 0.0182
Structure solution	SHELXT
Structure refinement	SHELXL
Refined parameters	40
Goodness of fit (χ^2)	1.197
$R1$ (all data); $R1$ [$F^2 > 2\sigma(F^2)$]	0.0210; 0.0177
$wR2$ (all data); $wR2$ [$F^2 > 2\sigma(F^2)$]	0.0344; 0.0335
$\Delta\rho_{max}$; $\Delta\rho_{min}$ [e Å^{-3}]	1.050, –1.327

$Sr_3P_6O_6N_8$, $Ba_3P_6O_6N_8$).[25,39–41] The corresponding O/N–P–O/N angles vary between 107.81(9) and 112.6(2)° and deviate only slightly from the regular tetrahedron angle and are also in good agreement with values known from literature. The crystal structure contains two crystallographically different Ba positions.

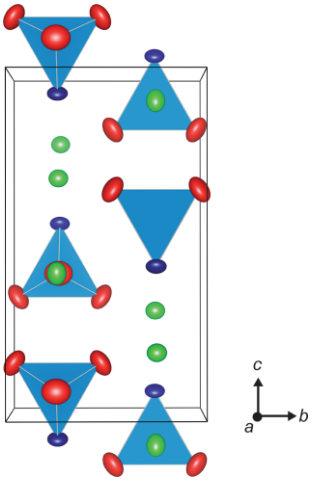

Figure 2. Crystal structure of Ba_2PO_3N along [001] with Ba atoms in green, O atoms in red, N atoms in blue and PO_3N tetrahedra in blue (displacement parameters with 90 % probability, drawings generated with VESTA).[42]

While Ba1 is coordinated by three N and seven O atoms, Ba2 is only surrounded by two N and seven O atoms (see Figure 3). The Ba–O [2.764(2)–3.131(2) Å] and Ba–N distances [2.731(3)-3.043(3) Å] are in the same range as already reported for other barium (oxo)nitridophosphates (e.g. $Ba_3P_6O_6N_8$, BaP_2N_4, $Ba_3P_5N_{10}X$).[41,43,44] Based on the obtained structure model from single-crystal X-ray diffraction, a Rietveld refinement of powder X-ray diffraction data was conducted in order to check phase purity. Thereby, a small amount of an unknown side phase, which is marked with asterisks in Figure 4, was observed. The washed product shows no evidence of residual mineralizers such as $NaNH_2$ or KNH_2. Table S7 and S8 in the Supporting Information summarize the crystallographic data.

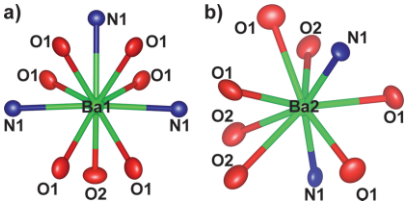

Figure 3. Coordination of Ba1 (a) and Ba2 (b) atoms in Ba_2PO_3N. Ba atoms are illustrated in green, O atoms in red and N atoms in blue (displacement parameters with 90 % probability, drawings generated with VESTA).[42]

Energy Dispersive X-ray Spectroscopy (EDX)

EDX measurements on Eu^{2+} doped Ba_2PO_3N samples (nominal concentration of ≈ 1 mol-% regarding to Ba) were carried out for chemical analysis and no elements other than the expected (Ba, P, O, and N) and trace amounts of Eu were detected. The obtained atomic ratio of Ba/P/O/N ≈ 2.1:1.0:2.5:0.9 is in good agreement with the sum formula of the title compound (Table S9, Supporting Information).

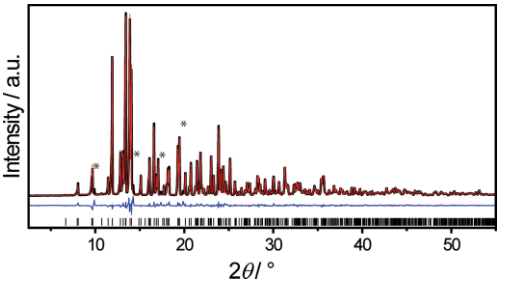

Figure 4. Rietveld refinement of PXRD data of Ba_2PO_3N with experimental data (black line), calculated diffraction pattern (red line), difference profile (blue line) and reflection positions of Ba_2PO_3N (black bars). Reflections of unknown side phases are marked with asterisks.

Fourier-Transform Infrared Spectroscopy (FTIR)

The exclusion of any NH_x functionality in Ba_2PO_3N was performed by FTIR spectroscopy. As no significant absorption bands appear in the region around 3000 cm^{-1} (Figure S2, Supporting Information), the absence of N-H groups in the crystal structure can be confirmed.[45] However, the broad and weak band between 2400 and 3400 cm^{-1} can be explained by partial surface hydrolysis of the sample, owed to the measuring method. The strong absorption bands in the region between 600 and 1400 cm^{-1} can be attributed to symmetric and asymmetric stretching modes of the P–N-framework and are similar to the absorption bands of Ca_2PO_3N and Sr_2PO_3N, indicating the structural similarity of these three compounds.[25]

UV/Vis Spectroscopy

In order to investigate the optical properties of Ba_2PO_3N, diffuse reflectance spectroscopy was conducted. The spectrum shows an absorption band around 250 nm (Figure S3, Supporting Information), which is in agreement with the white color of the sample. The Kubelka–Munk function $F(R) = (1 - R)^2/2R$, where R represents the reflectance, was used to calculate a pseudo-absorption spectrum.[46] The band gap was determined subsequently by drawing a tangent at the inflection point of the Tauc plot (see Figure 5), where $[F(R)\cdot h\nu]^{1/n}$ is plotted vs. $h\nu$, with n =

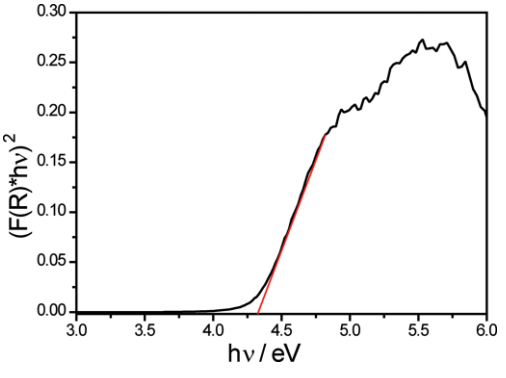

Figure 5. Tauc plot of Ba_2PO_3N (black line) with a tangent at the inflection point (red line).

1/2 assuming a direct transition.[47] The determined band gap is approximately 4.3 eV.

Luminescence

$Ba_2PO_3N:Eu^{2+}$ shows strong green emission upon irradiation with UV light (see Figure S4 in the Supporting Information). The excitation spectrum (see Figure 6) of a $Ba_2PO_3N:Eu^{2+}$ (≈ 1 at.-% Eu^{2+}) single crystal shows a maximum at 410 nm. Upon excitation (λ_{exc} = 420 nm), the title compound shows broad emission at λ_{em} = 534 nm with a full width at half-maximum (fwhm) of 85 nm/2961 cm^{-1}. The broad emission arises most likely from the two emission bands, due to two different Ba positions, which can be substituted by Eu^{2+}. The luminescence behavior is similar to that of isotypic $Ca_2PO_3N:Eu^{2+}$ and the oxosilicates $M_2SiO_4:Eu^{2+}$ (M = Ca, Sr, Ba) crystallizing in the β-K_2SO_4 structure type as well.[25,48] Furthermore, the emission wavelength of $Ba_2PO_3N:Eu^{2+}$ is similar to that of $SrP_2N_4:Eu^{2+}$ (λ_{em} = 529 nm), however, the emission is broader (fwhm = 2432 cm^{-1}).[43]

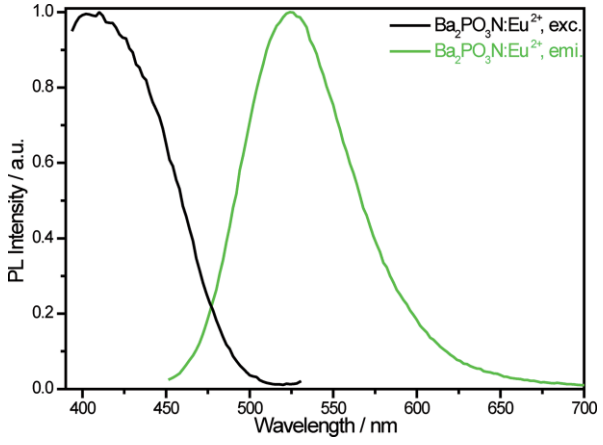

Figure 6. Excitation (black line) and emission (green line) spectra of $Ba_2PO_3N:Eu^{2+}$.

Low temperature measurements (λ_{exc} = 390 nm) between 6 and 300 K were conducted on thick-bed powder samples in order to investigate thermal quenching of $Ba_2PO_3N:Eu^{2+}$. For this purpose, the luminescence intensities were measured and integrated at different temperatures (Figure S5 in the Supporting Information). Figure 7 illustrates the thermal quenching of $Ba_2PO_3N:Eu^{2+}$, by decreasing the initial intensity (6 K) down to ≈ 40 % at room temperature. For this reason, no further measurements such as internal quantum efficiency or high-temperature measurements were conducted. The stronger thermal quenching of the title compound compared to the isotypic orthosilicates $(Ba,Sr)_2SiO_4:Eu^{2+}$ (λ_{em} ≈ 525 nm, fwhm ≈ 2420 cm^{-1})[48] that found practical application in solid-state lighting can be explained by the smaller optical band gap of the title compound (Ba_2SiO_4: E_g = 6.81 eV) that results in more pronounced non-radiative de-excitation of the activator ion via a photoionization process.[49] Additionally, the low temperature measurements reveal a second emission band, which is in accordance with the former mentioned presence of two substantially different Ba^{2+} sites. The observation of this second band, which is not obvious in the emission spectrum of the single crystal, might be traced back to the different excitation wavelengths or different activation energies of the two different excited Eu states towards photoionization.

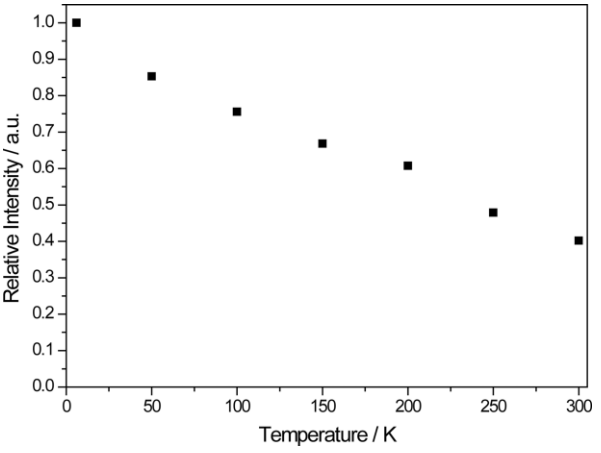

Figure 7. Thermal quenching data for $Ba_2PO_3N:Eu^{2+}$ at low temperatures (6–300 K).

Conclusions

The *ortho*-oxonitridophosphate Ba_2PO_3N was synthesized in supercritical ammonia starting from BaO, red phosphorus, KOH and NaN_3 at a temperature of 1070 K and a maximum pressure of 120 MPa using custom-built high-temperature autoclaves. KOH and NaN_3 act as ammonobasic mineralizers to increase the solubility of the other starting materials. In doing so, crystallites with sizes up to ≈ 600 µm grew on the wall at the upper part of the liner, which suggest a solution-based crystallization process via soluble intermediate species. The crystal structure was solved and refined from single-crystal X-ray diffraction. Ba_2PO_3N crystallizes in the β-K_2SO_4 structure type and is the first representative of an ammonothermally synthesized oxonitridophosphate with non-condensed PO_3N tetrahedra, expanding the degree of condensation range of ammonothermally accessible nitridophosphates to $1/4 \leq \kappa \leq 4/7$. The band gap was determined with diffuse reflectance spectroscopy to be 4.3 eV. Eu^{2+} doped samples show luminescence in the green region of the visible spectrum (λ_{em} = 534 nm, fwhm = 85 nm/2961 cm^{-1}) when excited with UV light (λ_{exc} = 420 nm). Low temperature measurements indicated strong thermal quenching even at room temperature, as only 40 % intensity remains compared to the intensity at 6 K. For future investigations, it would be interesting, if the ammonothermal method is applicable for synthesis of further *ortho*-(oxo)nitridophosphates and if the findings on ammonothermal (oxo)nitridophosphates in general could be transferred to other oxide or nitride systems such as (oxo)nitridosilicates.

Experimental Section

Due to moisture-sensitivity of the product, all manipulations were conducted under exclusion of oxygen and moisture in argon filled

gloveboxes (Unilab, MBraun, Garching, O_2 < 1 ppm, H_2O < 1 ppm). The filling of the autoclaves with ammonia was performed on a vacuum line (≤ 0.1 Pa) with argon and ammonia (both: Air Liquide, 99.999 %) supply. Washing treatments of the products were carried out in flame-dried Schlenk-type glassware connected to a vacuum line (≤ 0.1 Pa). All gases were further purified using gas purification cartridges [Micro Torr FT400–902 (for Ar) and MC400–702FV (for NH_3), SAES Pure Gas Inc., San Luis Obispo, CA, USA], providing a purity level of < 1 ppbV H_2O, O_2 and CO_2 (manufacturer's data).

Synthesis of $Eu(NH_2)_2$: $Eu(NH_2)_2$ was synthesized starting from Eu metal (99.99 %, smart elements) in supercritical ammonia according to the synthesis described in literature.[50]

Ammonothermal Synthesis: Ba_2PO_3N was synthesized ammonothermally starting from 0.75 mmol red P (23.2 mg, Merck, 99 %), 1.5 mmol BaO (230 mg, Alfa Aesar, 99.5 %), 0.75 mmol KOH (42.1 mg, Merck, 90 %) and 0.75 mmol NaN_3 (48.8 mg, Sigma-Aldrich, 99.5 %). In order to obtain Eu^{2+} doped samples, 0.015 mmol $Eu(NH_2)_2$ (3 mg) were added to the reaction mixture. All starting materials were ground in an agate mortar and transferred into a tantalum liner to protect the sample from autoclave impurities. After placing the liner in a Haynes® 282® autoclave (nickel based super-alloy, max. 1100 K, 170 MPa, 10 mL), the later was sealed via flange joints using a silver coated Inconel® 718 ring (GFD seals). The autoclave body is connected to a hand valve (SITEC) by an Inconel® 718 high-pressure tube. The hand valve contains a pressure transmitter (HBM P2VA1/5000 bar) and a bursting disk (SITEC). The assembled autoclave was evacuated, cooled to 198 K using an ethanol/liquid nitrogen mixture and filled with NH_3 (≈ 3.0 mL). The amount of NH_3 was determined using a mass flow meter (D-6320-DR, Bronkhorst, Ruurlo, Netherlands). After filling, the autoclave was heated within 2 h to 670 K and held at this temperature for 16 h, then heated to 1070 K within 3 h and held for 72 h reaching a maximum pressure of 120 MPa. Subsequently, the autoclave was cooled down and residual NH_3 was removed. The white (Ba_2PO_3N) and yellow ($Ba_2PO_3N:Eu^{2+}$) products were removed and washed with dry ethanol and dried under vacuum. Irregularly shaped single crystals of the product with sizes up to several hundred of µm grew on the wall of the liner.

Single-Crystal X-ray Diffraction: For single-crystal XRD measurements, $Ba_2PO_3N:EU^{2+}$ single crystals were placed and sealed in glass capillaries (Hilgenberg GmbH) under argon atmosphere. A Bruker D8 Quest diffractometer with Mo-K_α radiation (λ = 0.71073 Å) was used for data collection. The software package APEX3 was used for indexing and integration.[51,52] Furthermore, APEX3 was used for semiempirical absorption corrections (SADABS) and space group determination.[52–54] The crystal structure was solved using the SHELXT algorithm and refined by full-matrix least-squares methods using WinGX with implemented SHELXL.[55,56]

CSD 1975933 (for Ba_2PO_3N) contains the supplementary crystallographic data for this paper. These data can be obtained free of charge from FIZ Karlsruhe.

Powder X-ray Diffraction: The ground product was placed and sealed in a glass capillary (d = 0.3 mm, Hilgenberg GmbH) in argon atmosphere for PXRD measurement. The measurement was conducted using a Stoe STADI P diffractometer with Mo-$K_{\alpha1}$ (λ = 0.71073 Å) radiation, Ge(111) monochromator and Mythen 1K detector in modified Debye–Scherrer geometry. The program TOPAS was used for Rietveld refinement of the measured data.[57]

Scanning Electron Microscopy: Single-crystal images as well as EDX measurements were conducted on a scanning electron microscope [Dualbeam Helios Nanolab G3 UC (FEI), equipped with an EDX detector (X-Max 80 SDD, Oxford instruments)]. For this purpose, the samples were placed on adhesive carbon pads. Coating of the samples with a conductive carbon film was performed with a high-vacuum sputter coater (BAL-TEC MED 020, Bal Tec A).

Fourier Transform Infrared Spectroscopy: A Perkin Elmer BX II FTIR spectrometer equipped with a DuraSampler Diamond ATR (attenuated total reflection) unit under exposure to air was used for collection of a FTIR spectrum of Ba_2PO_3N.

UV/Vis Spectroscopy: UV/Vis measurements were conducted using a Jasco V-650 UV/Vis spectrophotometer equipped with Czerny-Turner mount, photomultiplier tube detector and deuterium (190–350 nm)/halogen (330–900 nm) lamps as light sources to estimate the optical band gap of Ba_2PO_3N. For this purpose, a diffuse reflectance measurement of the sample at room temperature was performed.

Luminescence Measurements: Single crystals sealed in silica glass capillaries were used for investigation of the luminescence properties of $Ba_2PO_3N:Eu^{2+}$. A HORIBA Fluoromax4 spectrofluorimeter system, attached via optical fibers to an Olympus BX51 microscope was used for data collection (λ_{exc} = 420 nm).

Low-temperature measurements were conducted in the range from 300 to 6 K performed on a thick-bed powder layer using a fiber-coupled spectroscopy system containing a thermally stabilized LED light source and a fiber-optic spectrometer from Ocean Optics (HR2000+ES) in an evacuated cooling chamber (λ_{exc} = 390 nm). The samples was cooled via a liquid-He compressor system from Advance Research System Inc. (ARS4HW).

Acknowledgments

The authors want to thank Lisa Gamperl for EDX measurements and Arthur Haffner for single-crystal X-ray measurements (all at Department of Chemistry, LMU Munich) as well as the group of Prof. Dr. E. Schlücker (especially Anna Kimmel and Dr. Thomas Steigerwald) for fabrication of the autoclaves (FAU Erlangen-Nürnberg). Financial support by the Deutsche Forschungsgemeinschaft (DFG) within the research group "Chemistry and Technology of the Ammonothermal Synthesis of Nitrides" (FOR 1600), project SCHN377/16-2, is gratefully acknowledged.

Keywords: Ammonothermal synthesis · Oxonitridophosphates · Luminescence · Supercritical fluids · Nitrides

[1] R. Juza, H. Jacobs, *Angew. Chem. Int. Ed. Engl.* **1966**, *5*, 247; *Angew. Chem.* **1966**, *78*, 208.
[2] H. Jacobs, U. Fink, *J. Less-Common Met.* **1979**, *63*, 273–286.
[3] H. Jacobs, J. Kockelkorn, J. Birkenbeul, *J. Less-Common Met.* **1982**, *87*, 215–224.
[4] D. Peters, H. Jacobs, *J. Less-Common Met.* **1989**, *146*, 241–249.
[5] T. Brokamp, H. Jacobs, *J. Alloys Compd.* **1992**, *183*, 325–344.
[6] H. Jacobs, E. von Pinkowski, *J. Less-Common Met.* **1989**, *146*, 147–160.
[7] T. Richter, R. Niewa, *Inorganics* **2014**, *2*, 29–78.
[8] J. Häusler, W. Schnick, *Chem. Eur. J.* **2018**, *24*, 11864–11879.
[9] R. Dwilinski, A. Wysmolek, J. Baranowski, M. Kaminska, R. Doradziński, H. Jacobs, *Acta Phys. Pol. A* **1995**, *88*, 833–836.
[10] R. Dwiliński, R. Doradziński, J. Garczyński, L. Sierzputowski, R. Kucharski, M. Zając, M. Rudziński, R. Kudrawiec, W. Strupiński, J. Misiewicz, *Phys. Status Solidi A* **2011**, *208*, 1489–1493.
[11] S. Pimputkar, S. Kawabata, J. S. Speck, S. Nakamura, *J. Cryst. Growth* **2014**, *403*, 7–17.

[12] J. Hertrampf, P. Becker, M. Widenmeyer, A. Weidenkaff, E. Schlücker, R. Niewa, *Cryst. Growth Des.* **2018**, *18*, 2365–2369.
[13] J. Häusler, S. Schimmel, P. Wellmann, W. Schnick, *Chem. Eur. J.* **2017**, *23*, 12275–12282.
[14] J. Häusler, R. Niklaus, J. Minár, W. Schnick, *Chem. Eur. J.* **2018**, *24*, 1686–1693.
[15] M. Mallmann, R. Niklaus, T. Rackl, M. Benz, T. G. Chau, D. Johrendt, J. Minár, W. Schnick, *Chem. Eur. J.* **2019**, *25*, 15887–15895.
[16] J. Häusler, L. Neudert, M. Mallmann, R. Niklaus, A.-C. L. Kimmel, N. S. A. Alt, E. Schlücker, O. Oeckler, W. Schnick, *Chem. Eur. J.* **2017**, *23*, 2583–2590.
[17] J. Häusler, L. Eisenburger, O. Oeckler, W. Schnick, *Eur. J. Inorg. Chem.* **2018**, 759–764.
[18] N. Cordes, T. Bräuniger, W. Schnick, *Eur. J. Inorg. Chem.* **2018**, 5019–5026.
[19] H. Jacobs, R. Nymwegen, *Z. Anorg. Allg. Chem.* **1997**, *623*, 429–433.
[20] M. Mallmann, C. Maak, R. Niklaus, W. Schnick, *Chem. Eur. J.* **2018**, *24*, 13963–13970.
[21] M. Mallmann, S. Wendl, W. Schnick, *Chem. Eur. J.* **2020**, *26*, 2067–2072.
[22] S. D. Kloß, W. Schnick, *Angew. Chem. Int. Ed.* **2019**, *58*, 7933–7944; *Angew. Chem.* **2019**, *131*, 8015–8027.
[23] W. Schnick, J. Luecke, *J. Solid State Chem.* **1990**, *87*, 101–106.
[24] D. Baumann, W. Schnick, *Eur. J. Inorg. Chem.* **2015**, 617–621.
[25] A. Marchuk, P. Schultz, C. Hoch, O. Oeckler, W. Schnick, *Inorg. Chem.* **2016**, *55*, 974–982.
[26] S. D. Kloß, N. Weidmann, W. Schnick, *Eur. J. Inorg. Chem.* **2017**, 1930–1937.
[27] A. P. Black, K. A. Denault, J. Oró-Solé, A. R. Goñi, A. Fuertes, *Chem. Commun.* **2015**, *51*, 2166–2169.
[28] Y.-S. Tang, S.-F. Hu, C. C. Lin, N. C. Bagkar, R.-S. Liu, *Appl. Phys. Lett.* **2007**, *90*, 151108.
[29] F. Golinski, H. Jacobs, *Z. Anorg. Allg. Chem.* **1994**, *620*, 965–968.
[30] H. Jacobs, R. Kirchgässner, *Z. Anorg. Allg. Chem.* **1990**, *581*, 125–134.
[31] H. Jacobs, S. Pollok, F. Golinski, *Z. Anorg. Allg. Chem.* **1994**, *620*, 1213–1218.
[32] R. Hoppe, *Angew. Chem. Int. Ed. Engl.* **1966**, *5*, 95–106; *Angew. Chem.* **1966**, *78*, 52–63.
[33] R. Hoppe, *Angew. Chem. Int. Ed. Engl.* **1970**, *9*, 25–34; *Angew. Chem.* **1970**, *82*, 7–16.
[34] R. Hübenthal, Maple, Program for the Calculation of MAPLE values, version 4; University of Gießen, Germany, **1993**.
[35] W. H. Baur, *Crystallogr. Rev.* **1987**, *1*, 59–83.
[36] I. D. Brown, D. Altermatt, *Acta Crystallogr., Sect. B* **1985**, *41*, 244–247.
[37] N. E. Brese, M. O'Keeffe, *Acta Crystallogr., Sect. B* **1991**, *47*, 192–197.
[38] R. Hoppe, S. Voigt, H. Glaum, J. Kissel, H. P. Müller, K. Bernet, *J. Less-Common Met.* **1989**, *156*, 105–122.
[39] S. J. Sedlmaier, E. Mugnaioli, O. Oeckler, U. Kolb, W. Schnick, *Chem. Eur. J.* **2011**, *17*, 11258–11265.
[40] S. J. Sedlmaier, J. Schmedt auf der Günne, W. Schnick, *Dalton Trans.* **2009**, 4081–4084.
[41] S. J. Sedlmaier, D. Weber, W. Schnick, *Z. Kristallogr. New Cryst. Struct.* **2012**, *227*, 1–2.
[42] K. Momma, F. Izumi, *J. Appl. Crystallogr.* **2011**, *44*, 1272–1276.
[43] F. J. Pucher, A. Marchuk, P. J. Schmidt, D. Wiechert, W. Schnick, *Chem. Eur. J.* **2015**, *21*, 6443–6448.
[44] A. Marchuk, S. Wendl, N. Imamovic, F. Tambornino, D. Wiechert, P. J. Schmidt, W. Schnick, *Chem. Mater.* **2015**, *27*, 6432–6441.
[45] S. Wendl, W. Schnick, *Chem. Eur. J.* **2018**, *24*, 15889–15896.
[46] R. López, R. Gómez, *J. Sol-Gel Sci. Technol.* **2012**, *61*, 1–7.
[47] J. Tauc, R. Grigorovici, A. Vancu, *Phys. Status Solidi B* **1966**, *15*, 627–637.
[48] T. L. Barry, *J. Electrochem. Soc.* **1968**, *115*, 1181–1184.
[49] P. Dorenbos, *J. Phys. Condens. Matter* **2005**, *17*, 8103–8111.
[50] M. Mallmann, J. Häusler, N. Cordes, W. Schnick, *Z. Anorg. Allg. Chem.* **2017**, *643*, 1956–1961.
[51] *SAINT*, Data Integration Software, Madison, Wisconsin, USA, **1997**.
[52] *APEX 3*, Vers. **2016**.2015–2010, Bruker-AXS, Karlsruhe, **2016**.
[53] G. M. Sheldrick, *SADABS, Multi-Scan Absorption Correction, v.2*, Bruker-AXS, Madison, WI, USA, **2012**.
[54] *XPREP Reciprocal Space Exploration*, Vers. 6.12, Bruker-AXS, Karlsruhe, **2001**.
[55] G. M. Sheldrick, *Acta Crystallogr., Sect. A* **2015**, *71*, 3–8.
[56] G. M. Sheldrick, *Acta Crystallogr., Sect. C* **2015**, *71*, 3–8.
[57] A. Coelho, *TOPAS Academic, Version 6*, Coelho Software, Brisbane (Australia), **2016**.

Received: January 15, 2020